MODIS-Derived Spatially Complete Surface Albedo Products: Spatial and Temporal Pixel Distribution and Zonal Averages

ERIC G. MOODY*
RS Information Systems, Inc., Lanham, Maryland

MICHAEL D. KING
Earth Sciences Division, NASA Goddard Space Flight Center, Greenbelt, Maryland

CRYSTAL B. SCHAAF
Center for Remote Sensing, Department of Geography, Boston University, Boston, Massachusetts

STEVEN PLATNICK
Earth Sciences Division, NASA Goddard Space Flight Center, Greenbelt, Maryland

(Manuscript received 5 June 2007, in final form 19 February 2008)

ABSTRACT

Five years (2000–04) of spatially complete snow-free land surface albedo data have been produced using high-quality-flagged diffuse bihemispherical (white sky) and direct-beam directional hemispherical (black sky) land surface albedo data derived from observations taken by the Moderate-Resolution Imaging Spectroradiometer (MODIS) instrument aboard the NASA *Terra* satellite platform (MOD43B3, collection 4). In addition, a spatially complete snow-free aggregate albedo climatological product was generated. These spatially complete products were prepared using an ecosystem-dependent temporal interpolation technique that retrieves missing data within 3%–8% error. These datasets have already been integrated into research and operational projects that require snow-free land surface albedo. As such, this paper provides details regarding the spatial and temporal distribution of the filled versus the original MOD43B3 data. The paper also explores the intra- and interannual variation in the 5-yr data record and provides a qualitative comparison of zonal averages and annual cycles of the filled versus the original MOD43B3 data. The analyses emphasize the data's inter- and intraannual variation and show that the filled data exhibit large- and small-scale phenological behavior that is qualitatively similar to that of the original MOD43B3. These analyses thereby serve to showcase the inherent spectral, spatial, and temporal variability in the MOD43B3 data as well as the ability of the fill technique to preserve these unique regional and pixel-level phenological characteristics.

1. Introduction

Surface albedo represents the ratio of reflected to incoming solar radiation at the earth's surface and is a central element in the determination and partitioning of the surface energy balance components. Surface albedo is also important for remote sensing of clouds (King et al. 1992, 2003, 2004; Platnick et al. 2003) and the determination of aerosol optical properties (Kaufman et al. 1997; King et al. 1999; Hsu et al. 2004) from satellite and airborne platforms, as well as from surface-based sun/sky radiometers (Holben et al. 1998; Dubovik et al. 2000).

Snow-free albedo is especially important for biophysically based land surface models that compute the exchange of energy, water, momentum, and carbon for various land use categories (Sellers et al. 1996; Ingram et al. 1989; Dirmeyer and Shukla 1994; Whitlock et al. 1995; Bounoua et al. 2002). In part in response to this need, validated (Liang et al. 2002; Jin et al. 2003a,b; Wang et al. 2004, Zhang et al. 2007) diffuse bihemispherical (white sky) and direct-beam directional hemispherical (black sky) land surface albedo data, known

* Current affiliation: Wyle Information Systems, McLean, Virginia.

Corresponding author address: Eric G. Moody, Wyle Information Systems, 1651 Old Meadow Rd., McLean, VA 22102.
E-mail: eric.g.moody@gmail.com

DOI: 10.1175/2008JAMC1795.1

as MOD43B3 (Schaaf et al. 2002), have been derived from observations taken by the Moderate-Resolution Imaging Spectroradiometer (MODIS) on the National Aeronautics and Space Administration (NASA) *Terra* (King and Herring 2000) spacecraft. Beginning on 24 February 2000, global values at 1-km spatial resolution were produced every 16 days for the first seven MODIS bands (0.47–2.1 μm) and for three broadband spectral regions (0.3–0.7, 0.3–5.0, and 0.7–5.0 μm).

However, roughly 30% of the global land surface, on an annual equal-angle basis, is obscured by persistent and transient cloud cover, and another 20% is obscured by ephemeral and seasonal snow cover. Therefore, a regionally consistent phenologically based temporal interpolation technique was developed to provide spatially complete global snow-free land surface albedo. This phenological technique fills missing, lower-quality-flagged, and snow-covered data from the original MOD43B3 dataset with temporally interpolated best estimates that have an accuracy of 3%–8% [see section 2 and Moody et al. (2005) for details].

Since the publication of Moody et al. (2005), the authors have slightly refined the technique (section 2) and have applied it to the five individual years of collection-4 MOD43B3 albedo data spanning 2000–04. In addition, MOD43B3 data from the same period were aggregated and treated using the same technique to produce a 5-yr albedo "climatology." These datasets have had success and are being used in research and operational projects that require interannually variable and spatially complete ephemeral and seasonal snow-free land surface albedo (Hsu et al. 2004, 2006; Marshak et al. 2006; Matsui et al. 2007; Ramon and Santer 2005; Roy et al. 2006; Tegen et al. 2006; Wen et al. 2006; Yu et al. 2006).

The purpose of this paper is therefore twofold. First, it gives users ample details on the spatial and temporal distributions of filled versus original MOD43B3 data (section 3). Second, it builds upon previous analysis (Moody et al. 2005) and presents seasonal albedo maps (section 4) as well as a qualitative comparison of zonally averaged fields and annual phenological cycles of pixels that have been filled versus pixels flagged as original high-quality MOD43B3 data (section 5). These analyses showcase the ability of the filling technique to preserve regional and pixel-level spatial, spectral, and temporal features that are inherent in the MOD43B3 data.

2. Collection-4 spatially complete albedo products

Collection-4 MOD43B3 data (2000–04) were processed using an enhanced version of the interpolation algorithm that was originally detailed in Moody et al. (2005). In brief, this temporal interpolation technique is predicated upon the establishment of a phenological curve for each pixel. When the phenological behavior of a pixel cannot be confidently determined, additional spatial support is introduced through the concept that within a limited region pixels representing the same ecosystem species will exhibit similar phenological, or temporal, behavior. Variations in local climate, canopy density and structure, and soil conditions, however, will result in significant pixel-to-pixel differences in the relative magnitudes of the behavioral curves. Therefore, to maintain these spatial pixel-level variations in a temporal sense, the shape of the extant phenological curves in the near ecosystem region will be coupled with all the temporal data that do exist for that pixel to establish the complete phenological curve for that pixel.

It is imperative to appreciate that this filling technique is not based primarily on land cover classes, but instead relies first and foremost on the establishment of robust temporal or phenological curves at each pixel location. Only as a last resort does the technique rely explicitly on the temporal information of local pixels of the same ecosystem class. This fallback approach is only used for a relatively small number of pixels globally—namely, in high-latitude regions impacted by ephemeral and seasonal snow and in tropical persistent-cloud regions.

To be more explicit, in these last-resort situations, local pixel-level statistics of the same ecosystem class are selectively introduced to enhance spatial fidelity and to provide robust temporal trends. Local-level statistics alone are only used in severely underrepresented circumstances, such as a locality in Cameroon where, because of the persistent clouds, no high-quality observations were retrieved for an entire year. Although the fallback approach maintains the unique interannual magnitude of each pixel's temporal trend, the interannual temporal variability of these pixels may be reduced.

The algorithm for processing the collection-4 MOD43B3 data was enhanced by selectively introducing 5-yr aggregate statistics (in lieu of single-year statistics) into the fallback approach. In addition, an updated MODIS International Geosphere–Biosphere Programme ecosystem classification dataset (Friedl et al. 2002), referred to as product MOD12Q1 (collection 4: day 149, 2001), was employed to provide, among other benefits, improved classification of urban areas.

Processing of MOD43B3 data from 2000 also required special attention because data from the first 3 of the 23 sixteen-day periods (periods 001, 017, and 033) that compose a year were unavailable because the

Terra satellite was not yet operational. As an approximation, the 5-yr aggregate MOD43B3 data and statistics were substituted directly for these three missing periods.

Last, the 5-yr aggregate of high-quality-flagged MOD43B3 data was filled using the interpolation technique to provide a 5-yr average that can be used as an average year. Note that in Antarctica only data from 2002 were used when aggregating the 5-yr average.

3. Spatial and temporal distributions of filled versus original MOD43B3 data

The processing quality assurance (QA) of the spatially complete albedo product is a record of whether a pixel in the original MOD43B3 data was flagged as high quality and was thereby preserved or was filled using the temporal interpolation technique (Moody et al. 2005). With this QA information, the spatial and temporal distributions of filled versus MOD43B3 data can be explored to provide researchers with a general reference of when and where they might expect to be using filled data. It can also provide a sense of where there is better temporal coverage that will in turn provide better phenological information for the interpolation technique. Although each wavelength may have its own unique number and location of pixels filled, the variation between wavelengths is minor. Therefore, data from the 0.86-μm band are used here to illustrate these distributions.

To provide an overall sense of global yearly temporal coverage, Fig. 1 illustrates the number of 16-day periods during which a pixel has maintained its original MOD43B3 data. Figure 1a, the 5-yr aggregate climatology, shows dramatic improvements in the overall temporal coverage relative to the data from any single year (Figs. 1b–f). This is especially true in areas with limited or no coverage (ephemeral and seasonal snow-impacted or cloud-covered areas). This increase in temporal coverage can lead to improved descriptions of phenological behavior. Note again that Antarctica aggregate values were derived solely from data from 2002.

Figures 1b–f illustrate that there is a significant degree of interannual variability in the number and location of high-quality-flagged MOD43B3 retrievals. They also show that the single-year products will have limited temporal coverage in persistently cloudy regions (the tropics, Southeast Asia, and southern India) and the ephemeral and seasonally snow-impacted areas (especially the mid-to-high latitudes in the Northern Hemisphere) in which the snow-free dormant state is not always observed. In areas for which no observations are available during the entire year, statistics from the 5-yr aggregate climatology are used to replace the single-year statistics to boost interpolation performance (see section 2).

Global trends in spatial and temporal distributions of filled versus original MOD43B3 data for the 5-yr climatology and the five single-year products can be discerned from Figs. 2–4. These figures confirm that snow-impacted and seasonally or persistently cloudy areas have the largest number of filled pixels, whereas mid-latitude pixels predominantly retain their originality. The region with the best MOD43B3 data coverage is the 20°–40°S zone, a belt containing central and southern Australia, southern Africa, and south-central South America. This is partially because this region, with the exception of parts of South America and Africa, is composed of predominantly arid ecosystems (deserts and shrublands). For the aggregate climatology, this area consists of nearly all MOD43B3 data, with as little as a fraction of 1% containing filled pixels.

It is not a surprise to note that these figures also demonstrate that for either the 5-yr climatology or the single-year data the beginning and end of the year have the highest overall percentage of filled data because of the impact of ephemeral and seasonal snow. The middle of the year has the lowest percentage of filled data, with the majority of filled data being from tropical regions. In addition, for any 16-day period, the climatology has, on average, 10%–20% more MOD43B3 pixels than any single-year dataset. On an annual global basis, the climatology has 32% filled data as compared with 45%–50% filled data for any single-year product.

For ecosystems, the variability (not shown) in percentage filled is primarily due to varying climate and the global distribution of ecosystem classes. It is not surprising to find that arid classes (desert, closed shrubs, or permanent snow) require the least amount of filling, whereas classes predominantly in the tropics (evergreen broadleaf forest or wetlands) require the most filling. Of the forest classes, the deciduous broadleaf forest (DBF) has the best coverage, primarily because the majority of these pixels are located in the 50°–30°N and 10°–30°S latitude belts. The aggregate climatology dramatically improves the coverage of classes within the broader 50°–20°N and 10°–40°S latitude belts (DBF, cropland, crop mosaic, urban, savanna, grassland, and closed shrubs).

4. Inter- and intraannual temporal and spatial variability

Radiative properties of snow-free surfaces are primarily dependent on the ecosystem, the properties of ground and vegetation canopy, the soil condition, and local climatological conditions (Reed et al. 1994; Kaduk and Heimann 1996; Schwartz 1998; Schwartz and Reed

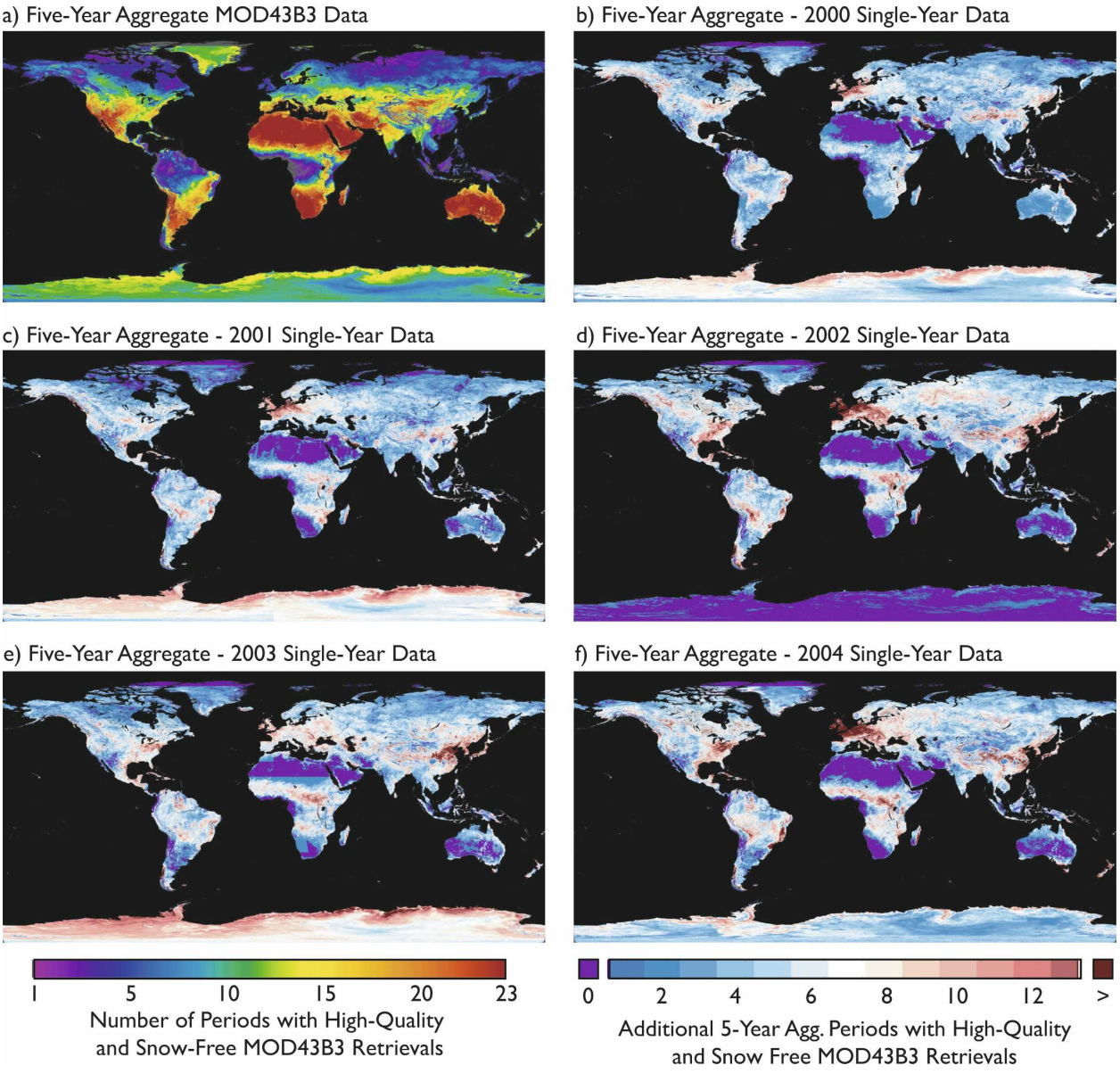

FIG. 1. Number of high-quality-flagged MOD43B3 retrievals preserved for each pixel in the spatially complete (a) 5-yr (2000–04) aggregate-climatology albedo data. For comparison, the differences between the climatology and single-year data for (b) 2000, (c) 2001, (d) 2002, (e) 2003, and (f) 2004 are shown. Midlatitude regions typically have more observations than do areas of persistent clouds (tropics) or ephemeral and seasonal snow and low illumination angles (high latitudes). By definition, the aggregate product provides more complete temporal information than does any single year of data.

1999; White et al. 1997; Zhang et al. 2003; Penuelas et al. 2004). Therefore, and as illustrated in Figs. 5–7, spatial and temporal variability in albedo arise from the global distribution of these factors and from seasonally changing climatological and growth conditions (often latitudinally correlated). In particular, vegetative surfaces exhibit defined and often dramatic phenological patterns. They can also exhibit curtailed or extended periods of productive vegetation due to interannual climatic variability; when examining Figs. 5–7, it is important to note that the averaging nature of the 5-yr aggregate does not provide for interannual variability.

It is instructive to begin by examining some trends in the aggregate maps (Fig. 5, left-hand side). In January (Fig. 5a), the Northern Hemisphere's vegetation is in full decay. Vegetation in southern North America, Europe, and Asia begins to grow during April (Fig. 5c) and reaches full maturity around midyear (Fig. 5e); grasslands and croplands in the Northern Hemisphere are especially bright in the near-infrared channel during

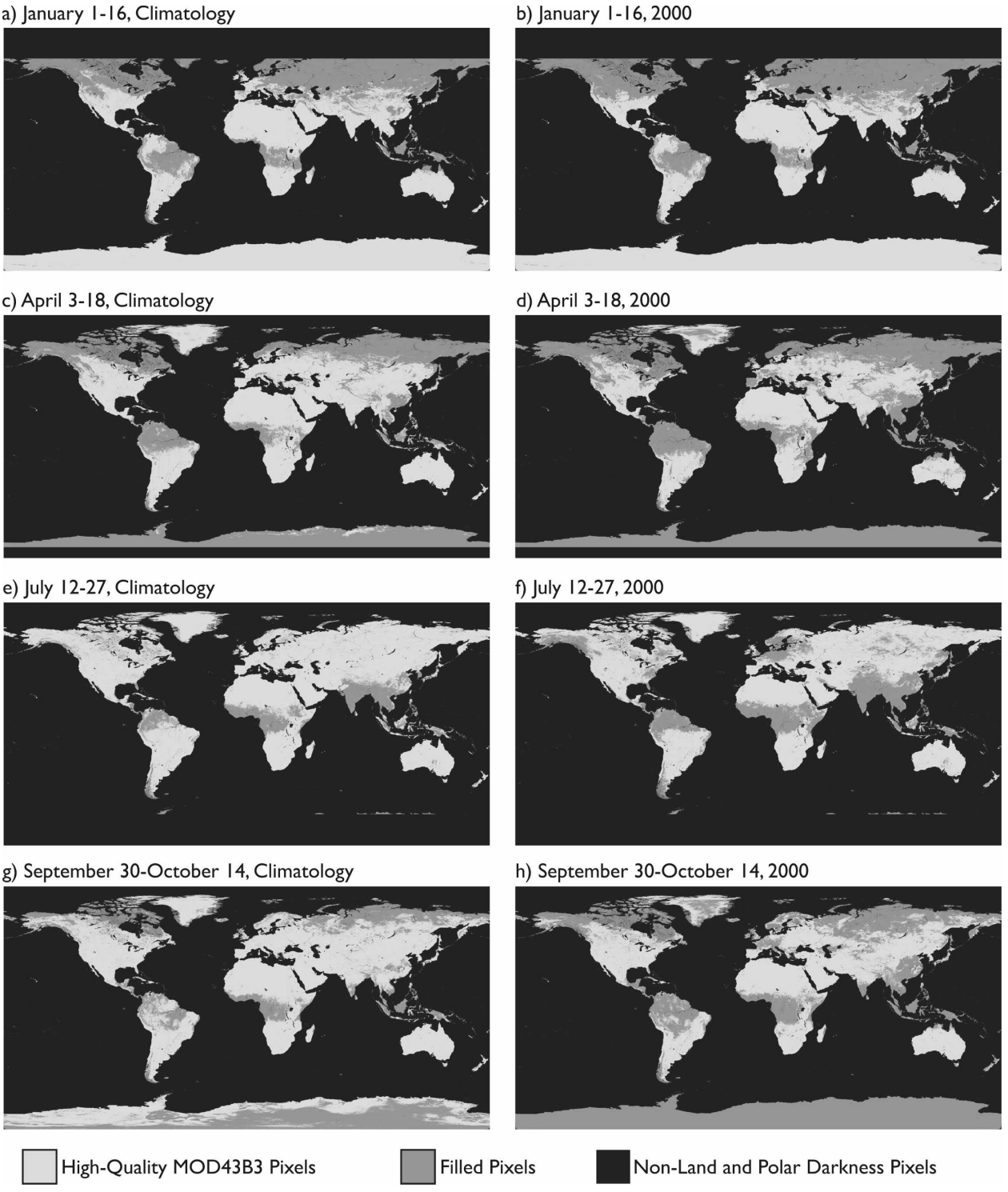

FIG. 2. Temporal and spatial distribution of preserved high-quality-flagged MOD43B3 retrievals and filled pixels at 0.86 μm for the 16-day periods of (a), (b) 1–16 Jan, (c), (d) 3–18 Apr, (e), (f) 12–27 Jul, and (g), (h) 30 Sep–14 Oct for (left) the five-year (2000–04) climatology and (right) the single-year albedo data for 2000.

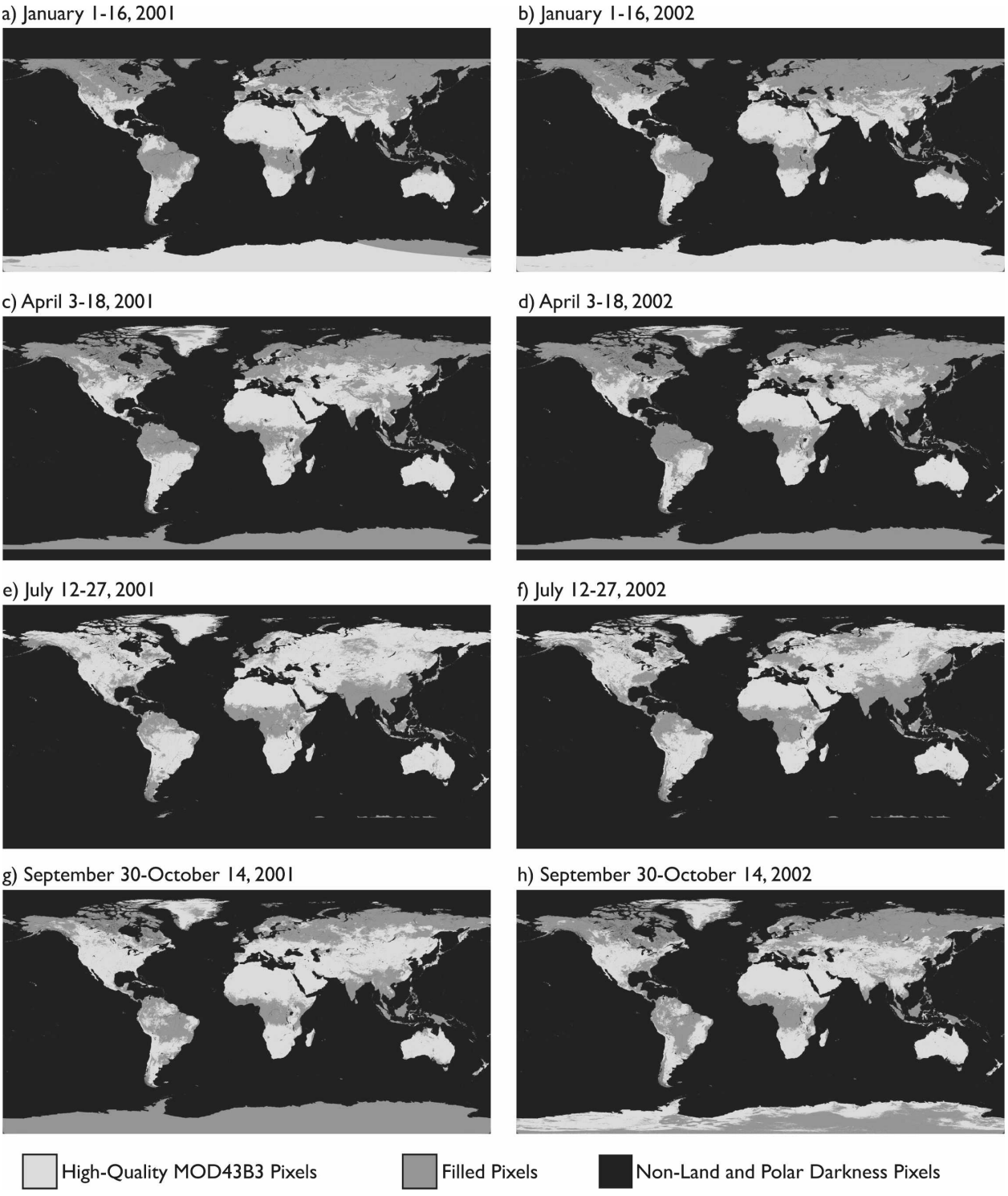

FIG. 3. As in Fig. 2, but with single-year (left) 2001 and (right) 2002 data.

July. The phenological cycle is completed as vegetation senesces during the later part of the year (Fig. 5g). The opposite trends hold for Southern Hemisphere vegetation over the course of the year.

It is also interesting to note the variability in 0.86-μm albedo values for regions (large and small) with the same ecosystem classification (see Fig. 5, left-hand side). For example, west-central Australia is primarily

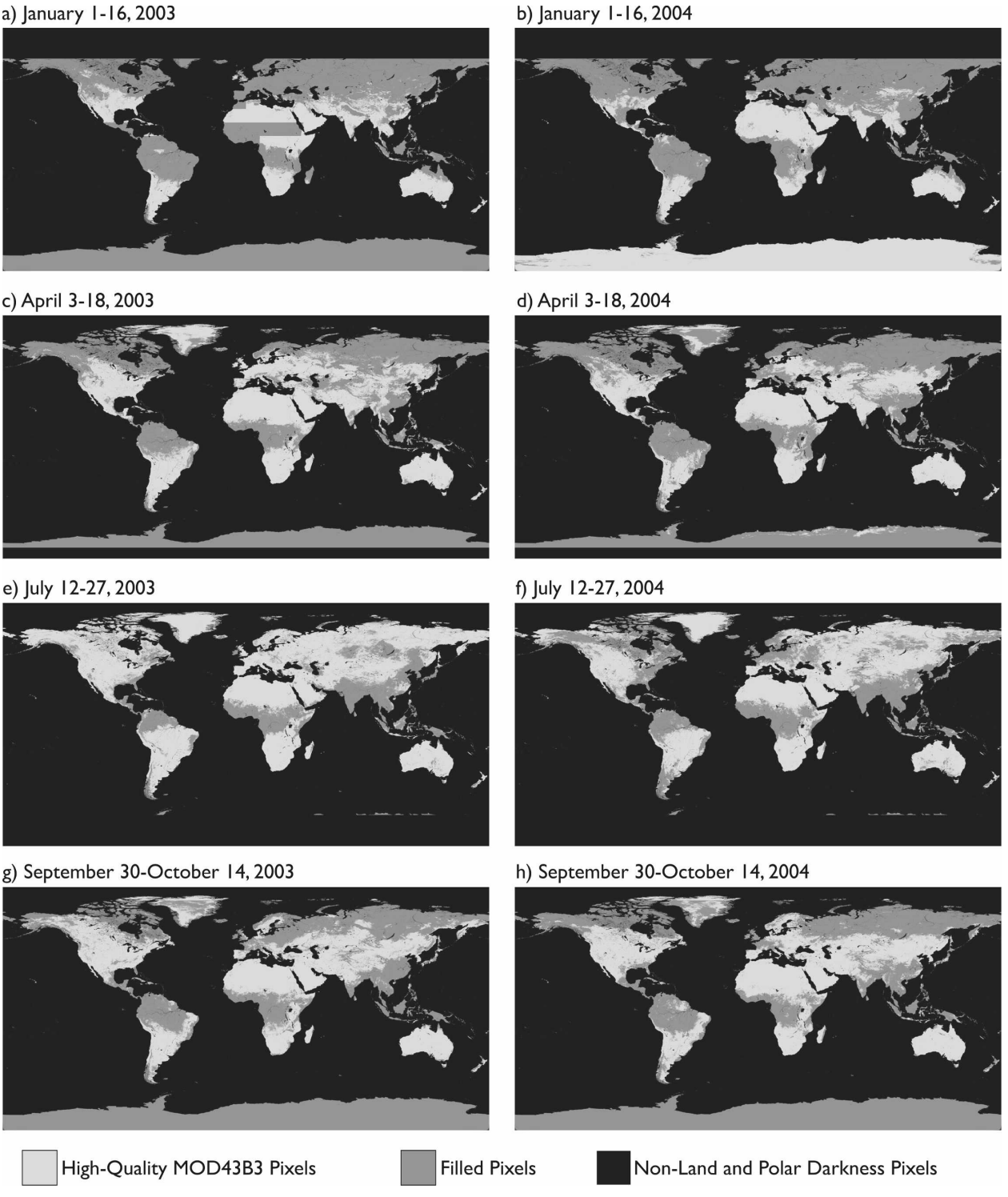

FIG. 4. As in Fig. 2, but with single-year (left) 2003 and (right) 2004 data.

open shrubland; however, varying vegetation types and/or levels of productivity cause the albedos to range between ~0.2 and 0.3. Varying soil conditions in the Sahara Desert cause similar speckled patterns. These local interecosystem variations can be especially pronounced in highly vegetated areas during growth or senescence states. For example, during April (Fig. 5c) croplands and grasslands in the midwestern United

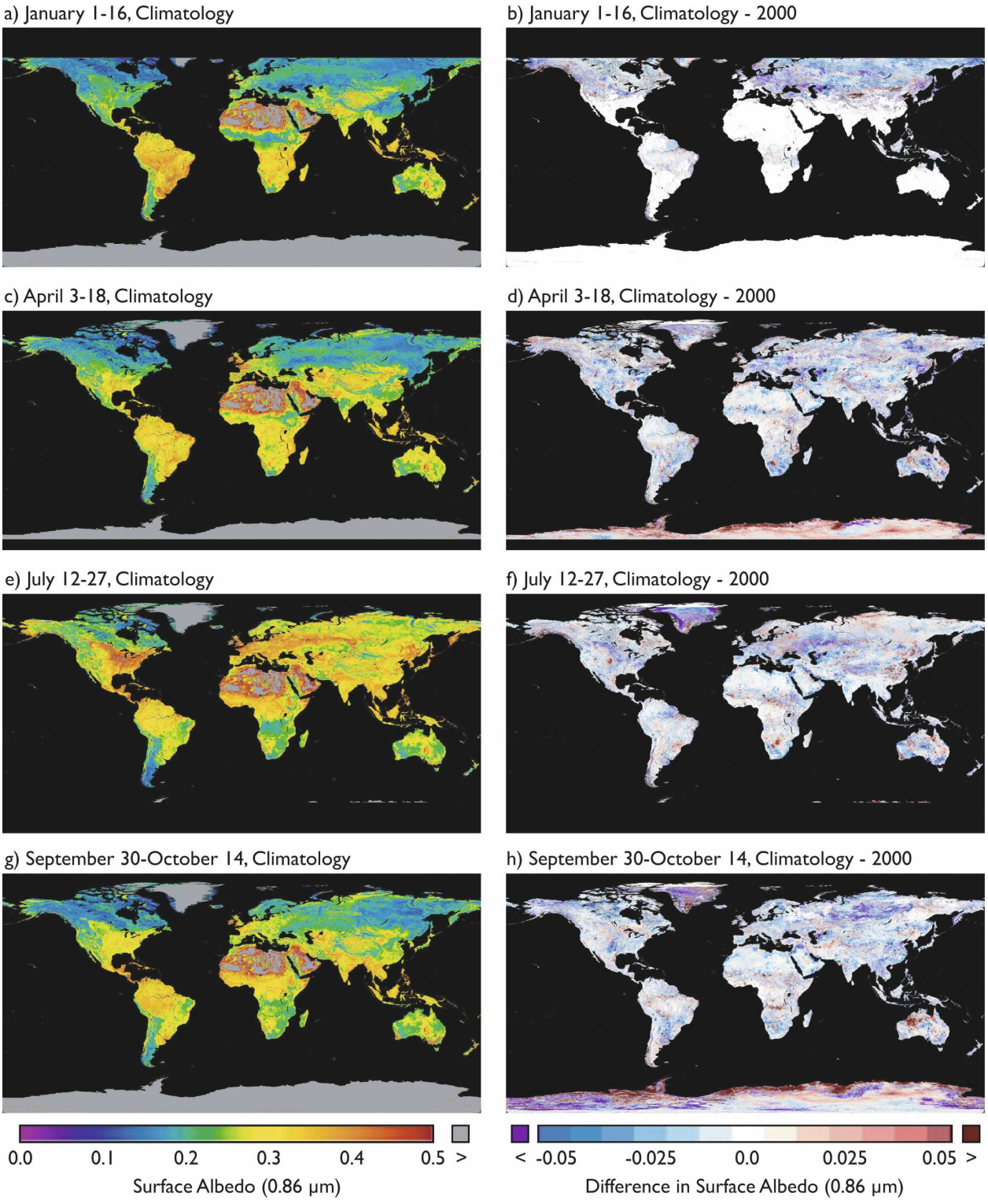

FIG. 5. (left) Spatially complete diffuse bihemispherical (white sky) albedo at 0.86 μm for data from the 5-yr (2000–04) climatology and (right) the difference between those data and single-year albedo data from 2000 for the 16-day periods of (a), (b) 1–16 Jan, (c), (d) 3–18 Apr, (e), (f) 12–27 Jul, and (g), (h) 30 Sep–14 Oct.

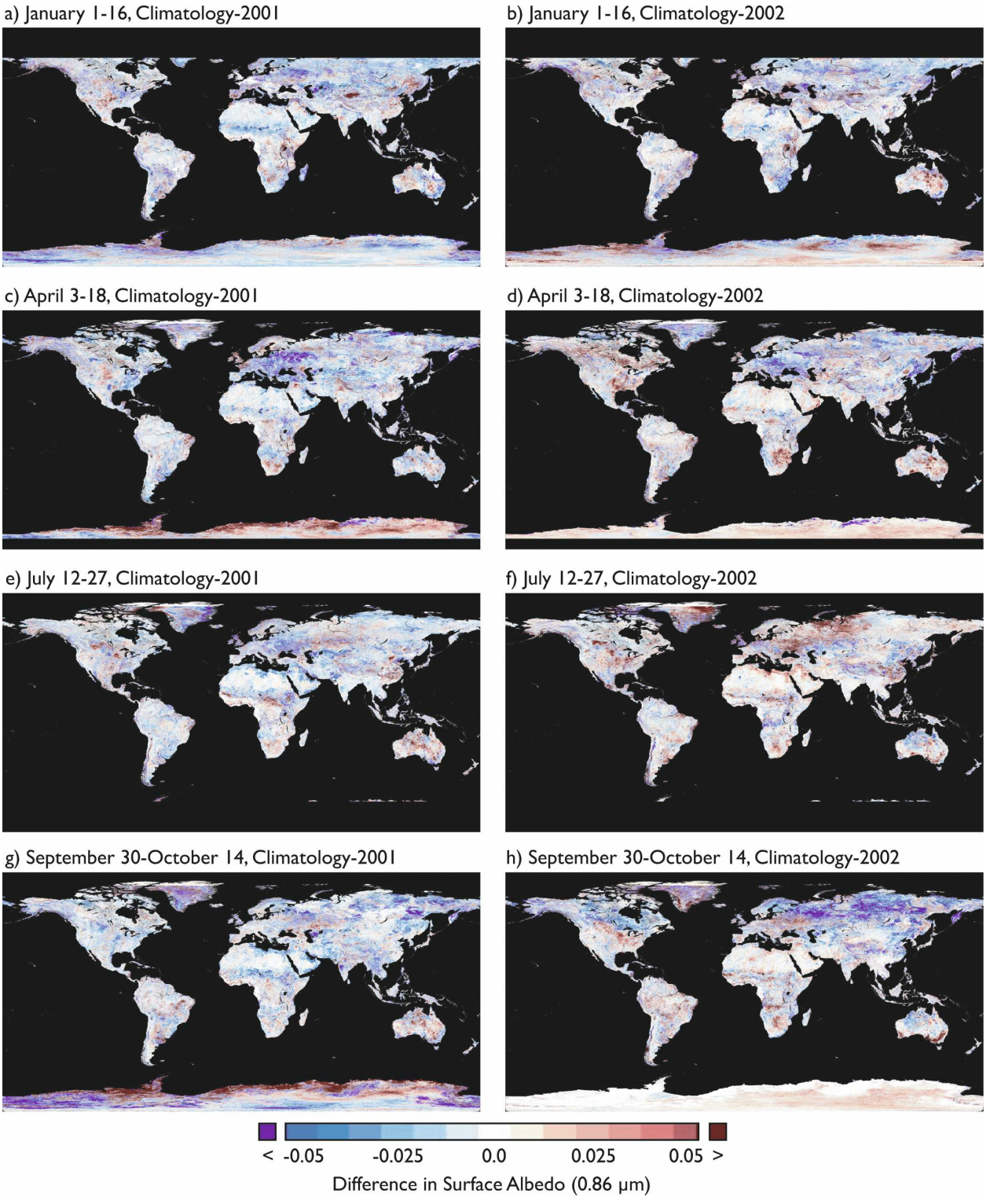

FIG. 6. As in Fig. 5, but for departures in albedo from the 5-yr (2000–04) climatology for single-year (left) 2001 and (right) 2002 albedo data.

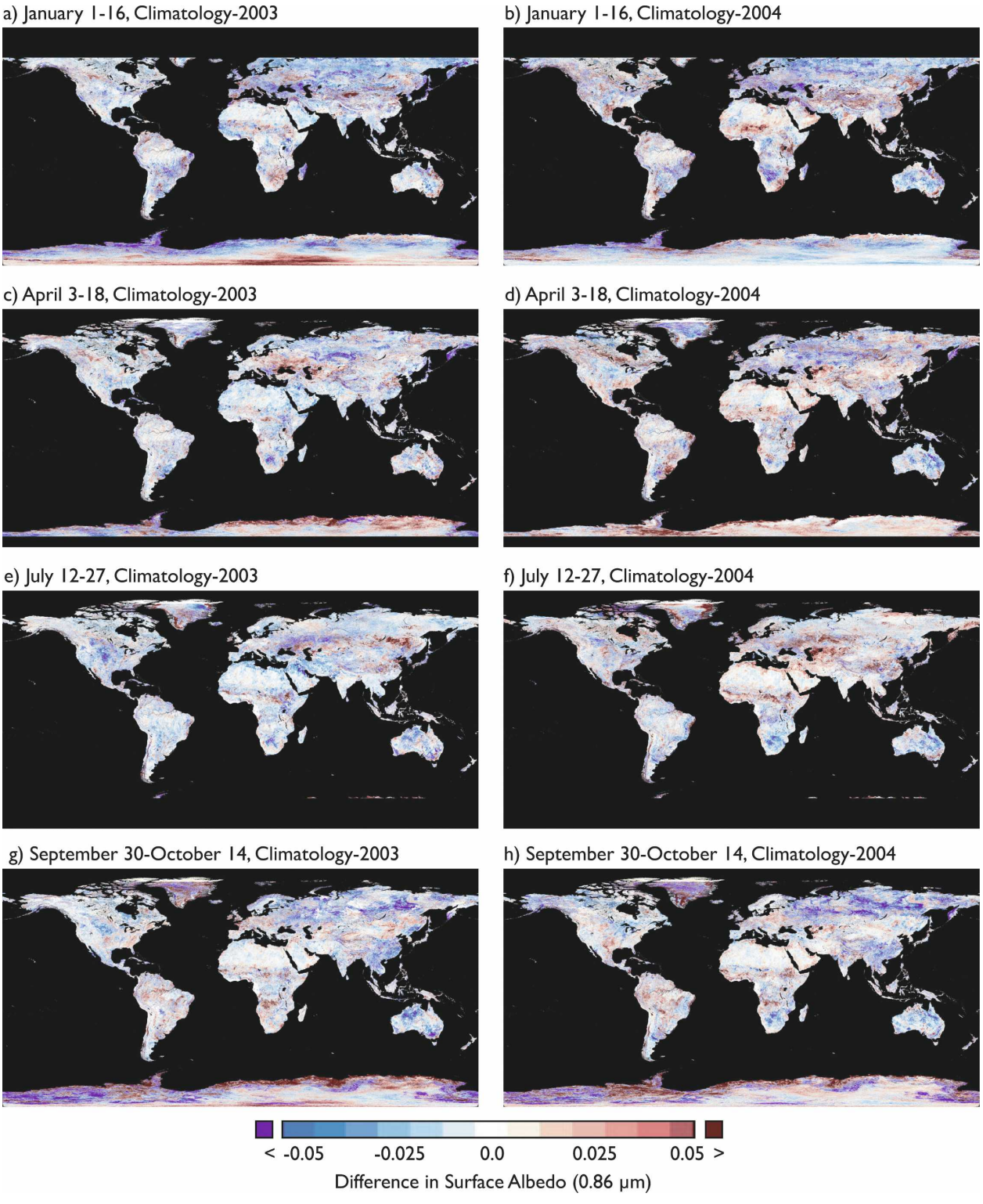

FIG. 7. As in Fig. 5, but for departures in albedo from the 5-yr (2000–04) climatology for single-year (left) 2003 and (right) 2004 albedo data.

States and Western Europe contain areas that have begun to grow while other local regions have not. This can most readily be seen in western Europe, where the vegetation in the United Kingdom and northwestern France has begun to grow even though in surrounding regions it has not.

One can also observe the movement of the ITCZ in the plots on the left-hand side of Fig. 5. As the ITCZ moves into a region, its associated rainfall provides conditions suitable for vegetative growth, which thereby produces increases in the 0.86-μm albedo. This trend can be readily seen as the ITCZ begins the year in Southern Africa, progresses northward through April, is in central Africa by midyear, and begins to make its way south during the later part of the year.

Interannual variability can be explored by comparing the differences between the 5-yr aggregate (Figs. 5a,c,e,h) and the single-year data (Figs. 5–7). For example, croplands in the midwestern United States during 2003 (left-hand side of Fig. 7) are not as bright as in the climatology, which may indicate a delayed growth cycle, or perhaps less productive vegetation; the opposite is true for certain midwestern regions the following year (2004; right-hand side of Fig. 7). In a similar way, examinations of Australia show substantial interannual variability.

5. Zonal averages and phenology of filled versus original MOD43B3 data

Even with the substantial variability of pixel-level, local, and regional phenological trends that arise from the factors presented in section 4, Moody et al. (2005) showed that their phenological interpolation technique could fill missing data within 3%–8% accuracy. This was accomplished by withholding existent data and testing the ability of the phenological curve to mimic these data. This overall error or uncertainty in the filled values is a highly convoluted mixture of various instrument, algorithm, and interpolation errors (number of observations, quality of MOD43B3 data, quality of the temporal information over the period, interannual variability in the number of observations and growth conditions, etc.). Despite this inability to directly propagate and identify sources of uncertainty, users can nevertheless gain an appreciation for the conditions under which the spatially complete product was generated by examining the accompanying processing QA information (described in section 3).

Further direct error analysis in global sense is not possible because the two data types (high-quality-flagged MOD43B3 and filled) are mutually exclusive and collectively exhaustive. In addition, alternative (i.e., non-MODIS) validation databases suffer from the same temporal and spatial coverage issues—namely, a lack of observations because of cloud or ephemeral snow coverage during the same periods.

Nonetheless, this paper seeks to build upon the previous error analysis by qualitatively comparing zonal averages and annual cycles of pixels that have been filled versus pixels flagged as high-quality MOD43B3 data. Such an analysis can showcase the ability of the filling technique to preserve pixel-level and regional spatial and temporal behavior that is inherent in the MOD43B3 data. For brevity, the analysis of the spatially complete products will be performed using one single year (2002) and the 5-yr climatological data. Although there are interannual variations among the single-year data, analysis of a single year of data will provide representative trends associated with the other years.

The authors chose to perform the analysis using diffuse bihemispherical (white sky) albedo because this represents reflectance under conditions of isotropic illumination and thereby excludes angular solar effects. To take into account the various factors (described in section 4) that cause variability in spatial and phenological behavior, the statistics were computed as ecosystem classification–dependent 10°-latitude zonal averages for every 16-day period. For conciseness and to provide trends over a range of albedo values and spectral characteristics, the authors chose to present statistics for three ecosystem classes (cropland, grassland, and mixed forest) and for three bands (0.47 and 0.86 μm and the shortwave broadband 0.3–5.0 μm). This section will continue with spatial (section 5a) and temporal (section 5b) trend discussions and will examine divergent trends (section 5c).

a. Zonal averages of filled versus high-quality-flagged MOD43B3 data

Figure 8 compares 10° latitudinal zonal averages in the single-year (2002) and the aggregate spatially complete albedo data for a single 16-day period (day 193, 12–27 July). For this time of year, there are few filled pixels in the 10°–40°S latitude belt: less than 10% filled pixels for single-year processing (2002) and less than 1% for the aggregate climatology. Conversely, the 0°–40°N latitude belts vary (by ecosystem) from roughly 40% to 90% filled pixels for the single-year processing (2002) and from 20% to 70% filled pixels from the aggregate climatology.

For the selected ecosystems and spectral bands, the filled and MOD43B3 pixels have trends that are qualitatively consistent. In the near-infrared 0.86-μm band, the cropland and mixed forest trends exhibit mature growth in the Northern Hemisphere and are dormant in

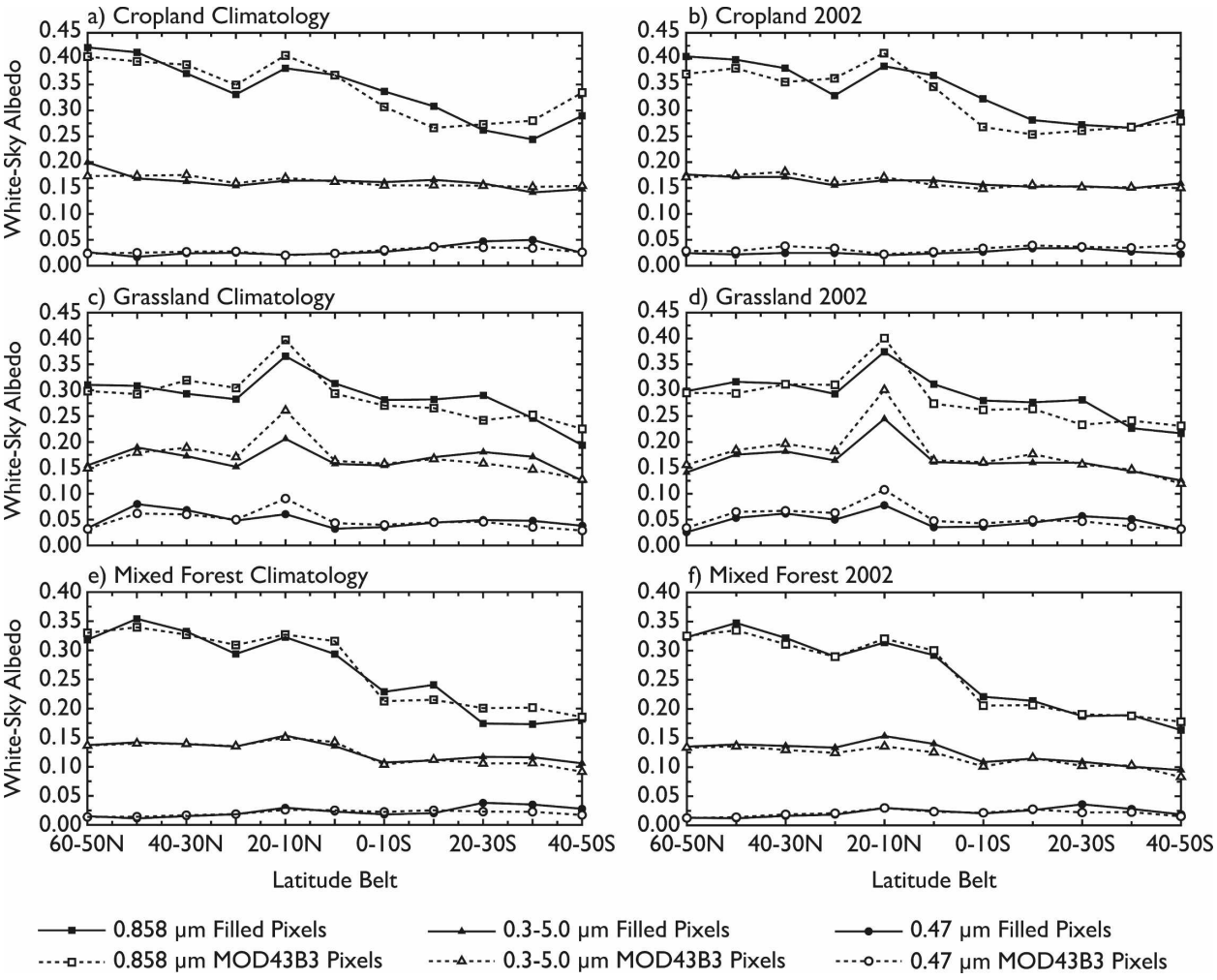

FIG. 8. Mean diffuse bihemispherical (white sky) albedo values computed by 10° latitude belts for three bands (0.47- and 0.86-μm narrowband and the 0.3–5.0-μm shortwave broadband) during the 16-day period of 12–27 Jul (data-day 193). Trends are computed for three ecosystem classes: (a), (b) cropland, (c), (d) grassland, and (e), (f) mixed forest from (left) the 5-yr aggregate climatology and (right) the 2002 single-year albedo data.

the Southern Hemisphere. The peak in the grassland occurs in the 20°–10°N latitude belt; the grasslands of this region are in full growth as the ITCZ brings rain to this region during this time of year.

Some slight divergences between trend lines are observed. Upon further analysis, detailed in section 5c, these departures arise when there are limited amounts of one type of data (either filled or MOD43B3). For example, in Fig. 8, some of the grassland MOD43B3 and filled data trends slightly diverge in the tropical to subtropical latitudes. This is primarily due to the limited number of filled pixels in this latitude belt. More specifically, in the 20°–10°N region, filled grassland pixels are located primarily in Africa, whereas MOD43B3 pixels are located primarily in the Americas. These regions have different vegetative types and conditions and thereby albedo values. This situation results in latitudinal mean values that diverge even though detailed comparisons of each region show agreement between MOD43B3 and filled data. Perhaps, in a counterintuitive way, these anomalies actually highlight the inherent spatial and temporal variability in the MOD43B3 data as well the ability of the fill method to provide values that preserve unique local, regional, and latitudinal phenology.

b. Phenological (temporal) behavior of filled versus high-quality-flagged MOD43B3 data

The phenological (temporal) behavior of the single-year (2002) and aggregate climatology data can most readily be examined by focusing on a single latitude belt; the 50°–40°N latitude belt was selected because its

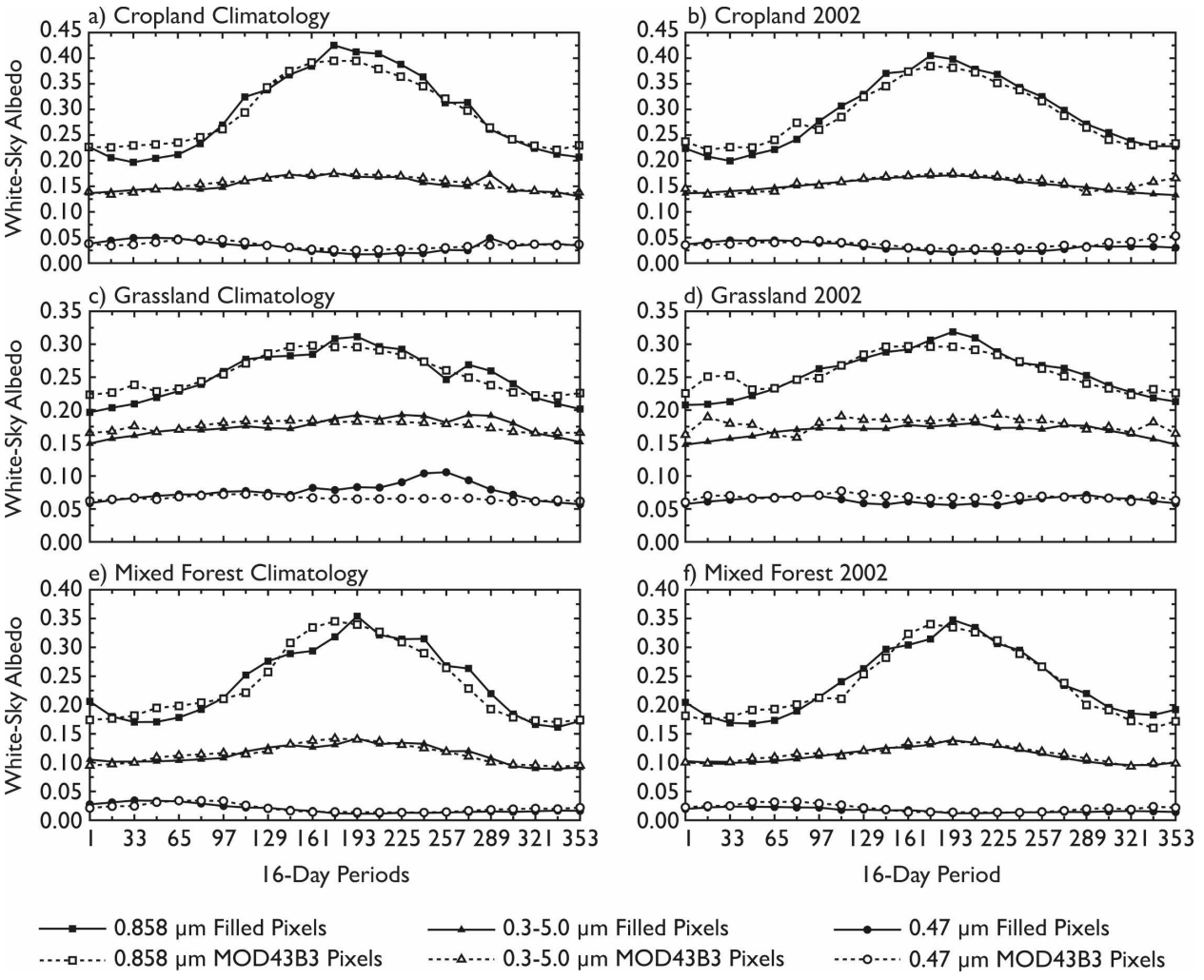

FIG. 9. As in Fig. 8, but for each 16-day period over the 50°–40°N latitude belt.

vegetation exhibits large differences in the mean albedo values of the vegetative mature and senescent states. Figure 9 shows 10° latitudinal mean diffuse bihemispherical (white sky) albedo as a function of 16-day time period for each of the 23 time periods and for three ecosystems.

The temporal trends show that the MOD43B3 and filled data exhibit qualitatively similar behavior, with the maximum vegetative growth and dormant states appearing to be qualitatively consistent (the 0.86-μm band best shows the vegetative trends) for both the single-year and aggregate climatology data. A closer inspection, however, reveals that there are some discrepancies. As detailed in section 5a and further in section 5c, these features arise from small sample sizes of MOD43B3 or filled pixels that are disproportionately distributed across the latitude belt. Although this situation has an impact on the latitudinal means, detailed analyses of local averages show that MOD43B3 and filled pixels have comparable values.

For example, during the dormant stages, grasslands from the 0.86-μm 2002 single-year processed data primarily consist of filled pixels. In examining Fig. 9d, it is seen that the trend for the MOD43B3 pixels in the beginning of the year differs from the trend of the filled pixels, with maximum deviation occurring near the 16-day period starting at day 17 (17 January). During this period, only 18.7% of the latitude belt's pixels are from original MOD43B3 data.

Upon closer inspection, a near majority (48.1%) of these MOD43B3 pixels are seen to be located in a single region located in eastern Asia. This region's dormant state has a white-sky albedo (0.278) that is higher than the spatially representative latitudinal average filled-pixel state (0.209). As such, the pixels from this area dominate the statistical computation, resulting in

differing mean latitudinal MOD43B3 and filled trends during this time of year. However, the averages of this region's filled (0.281) and MOD43B3 (0.278) pixels are comparable. During this same time period, the deviation in the aggregate-climatology data (Fig. 9c) is reduced. This is primarily due to there being more MOD43B3 data that are better distributed across the latitude belt. In all, this provides further evidence of the spatial and temporal variability inherent in the MOD43B3 data and the ability of the fill procedure to preserve these variations.

In a reverse situation, for the aggregate climatology's grassland 0.47-μm data (Fig. 9c) the filled and MOD43B3 trends differ between days 161 and 289 (peaking at day 257). During this time, the filled pixels represent only a fraction of 1% of the total grassland pixels in this latitude belt. In fact, at the peak deviation, day 257, there are only 4420 filled pixels, or about 0.25% of the total grassland pixels in the latitude belt. Of these 4420 filled pixels, 4263 pixels (96.4%) are located in a single, small region located in central Asia.

This region, however, has a filled-pixel average (0.106) that differs substantially from the spatially representative MOD43B3 latitudinal average albedo (0.066). As a result, the mean filled-pixel latitudinal trend deviates from the spatially representative MOD43B3 latitudinal trend during this time period. Upon closer inspection of this region, it is apparent that the MOD43B3 mean (0.113) is comparable to the filled-value mean (0.106). During this same time period, the deviation in the single-year data (Fig. 9d) is reduced as a result of there being more filled data that are better distributed across the latitude belt. This provides further evidence of the spatial and temporal variability inherent in the MOD43B3 data and the ability of the fill procedure to preserve these local variations.

In the final analysis, the qualitatively similar MOD43B3 and filled-pixel temporal trends showcase the ability of the fill technique to represent large scale trends properly. The deviations in trends, perhaps in a counterintuitive way, highlight both the inherent spatial and temporal variability in the MOD43B3 data as well the ability of the fill method to preserve the unique phenological state of each local and regional area.

c. *Influence of disproportionately distributed pixels on latitude-belt averages*

As seen in sections 5a and 5b, care must be taken when interpreting latitude-belt statistical trends because means can be skewed when contributions from regions within the latitude belt are not proportionally distributed; this scenario frequently occurs when there are relatively small numbers of either MOD43B3 or filled pixels (i.e., winter or summer; see Figs. 2–4). Then again, these occurrences provide the chance to showcase the spatial variability inherent in the MOD43B3 product and the ability of the fill technique to represent local behavior.

To explain this concept further, within a latitude belt an ecosystem's pixels are typically distributed across several landmasses, each of which has unique climatological characteristics, vegetative and ground conditions, and structure. Differences between the conditions of each region result in varying albedo magnitudes (dormant and mature) within the same ecosystem class, as seen in Figs. 5–7. With a sample that is proportionately distributed across a latitude belt, these local variances are dampened and a representative latitude-belt mean can be computed. However, when the sample is disproportionately distributed across a latitude belt, one or more regions can dominate the mean calculation, resulting in a nonrepresentative latitude-belt mean.

Small samples in which a single region is wholly over- or underrepresented can exacerbate this problem. Because regions (and pixels) have unique magnitudes (dormant or mature) that can vary substantially, a latitudinal mean computed from such a sample could be substantially different than if it had been computed from a proportionally distributed sample. On a positive note, these cases do provide excellent examples of the inherent MOD43B3 regional and pixel-level spatial and temporal variability. These cases also demonstrate the temporal interpolation technique's ability to preserve these inherent MOD43B3 behaviors.

6. Conclusions

In this paper, we describe refinements to the temporal interpolation technique that address areas of limited observation: namely, persistently cloudy (tropical) and ephemeral and seasonal snow-impacted (high latitude) regions. The refined algorithm is then applied to 5 yr (2000–04) of collection-4 MOD43B3 data. Also described is the creation of a spatially complete 5-yr aggregate climatological product that is free of ephemeral and seasonal snow. For this product, 5 yr (2000–04) of high-quality-flagged MOD43B3 observations were aggregated for each of the annual 23 16-day time periods. The remaining missing values were filled using the refined phenological interpolation technique.

This paper also provides additional details regarding the spatial and temporal distributions of the filled versus original MOD43B3 data. Seasonal albedo maps for the 5-yr and the aggregate product are provided. A qualitative comparison of temporal and spatial trends

of data that have been filled versus data flagged as original MOD43B3 values is provided. This study underscores the ability of the filling technique to preserve regional and pixel-level spatial, spectral, and temporal behavior that is inherent in the MOD43B3 data.

At the time of writing, single-year and multiyear climatological digital data from this analysis were available for public download at ftp://modis-atmos.gsfc.nasa.gov.

Acknowledgments. The research reported in this article was supported by the MODIS Science Team under NASA Contract 621-30-H4 to Goddard Space Flight Center (EGM, MDK, SP) and NASA Contract NAS5-31369 to Boston University (CBS). The authors express their appreciation to Dr. Bernard Pinty, European Commission Joint Research Centre, for insightful suggestions to clarify this work and to Dr. Lahouari Bounoua, NASA Goddard Space Flight Center, for providing valuable insight into modeling-community requirements and for reviewing the methods used in this work.

REFERENCES

Bounoua, L., R. DeFries, G. J. Collatz, P. Sellers, and H. Khan, 2002: Effects of land cover conversion on surface climate. *Climatic Change,* **52,** 29–64.

Dirmeyer, P. A., and J. Shukla, 1994: Albedo as a modulator of climate response to tropical deforestation. *J. Geophys. Res.,* **99,** 20 863–20 878.

Dubovik, O., A. Smirnov, B. N. Holben, M. D. King, Y. J. Kaufman, T. F. Eck, and I. Slutsker, 2000: Accuracy assessments of aerosol optical properties retrieved from Aerosol Robotic Network (AERONET) sun and sky radiance measurements. *J. Geophys. Res.,* **105,** 9791–9806.

Friedl, M. A., and Coauthors, 2002: Global land cover mapping from MODIS: Algorithms and early results. *Remote Sens. Environ.,* **83,** 287–302.

Holben, B. N., and Coauthors, 1998: AERONET—A federated instrument network and data archive for aerosol characterization: An overview. *Remote Sens. Environ.,* **66,** 1–16.

Hsu, N. C., S.-C. Tsay, M. D. King, and J. R. Herman, 2004: Aerosol properties over bright-reflecting source regions. *IEEE Trans. Geosci. Remote Sens.,* **42,** 557–569.

——, ——, ——, and ——, 2006: Deep blue retrievals of Asian aerosol properties during ACE-Asia. *IEEE Trans. Geosci. Remote Sens.,* **44,** 3180–3195.

Ingram, W. J., C. A. Wilson, and J. F. B. Mitchell, 1989: Modeling climate change: An assessment of sea ice and surface albedo feedbacks. *J. Geophys. Res.,* **94,** 8609–8622.

Jin, Y., C. B. Schaaf, F. Gao, X. Li, A. H. Strahler, W. Lucht, and S. Liang, 2003a: Consistency of MODIS surface bidirectional reflectance distribution function and albedo retrievals: 1. Algorithm performance. *J. Geophys. Res.,* **108,** 4158, doi:10.1029/2002JD002803.

——, ——, C. E. Woodcock, F. Gao, X. Li, A. H. Strahler, W. Lucht, and S. Liang, 2003b: Consistency of MODIS surface bidirectional reflectance distribution function and albedo retrievals: 2. Validation. *J. Geophys. Res.,* **108,** 4159, doi:10.1029/2002JD002804.

Kaduk, J., and M. Heimann, 1996: A prognostic phenology scheme for global terrestrial carbon cycle models. *Climate Res.,* **6,** 1–19.

Kaufman, Y. J., D. Tanré, L. A. Remer, E. F. Vermote, A. Chu, and B. N. Holben, 1997: Operational remote sensing of tropospheric aerosol over land from EOS Moderate Resolution Imaging Spectroradiometer. *J. Geophys. Res.,* **102,** 17 051–17 067.

King, M. D., and D. D. Herring, 2000: Monitoring Earth's vital signs. *Sci. Amer.,* **282,** 72–77.

——, Y. J. Kaufman, W. P. Menzel, and D. Tanré, 1992: Remote sensing of cloud, aerosol, and water vapor properties from the Moderate Resolution Imaging Spectrometer (MODIS). *IEEE Trans. Geosci. Remote Sens.,* **30,** 2–27.

——, ——, D. Tanré, and T. Nakajima, 1999: Remote sensing of tropospheric aerosols from space: Past, present, and future. *Bull. Amer. Meteor. Soc.,* **80,** 2229–2259.

——, and Coauthors, 2003: Cloud and aerosol properties, precipitable water, and profiles of temperature and humidity from MODIS. *IEEE Trans. Geosci. Remote Sens.,* **41,** 442–458.

——, S. Platnick, P. Yang, G. T. Arnold, M. A. Gray, J. C. Riedi, S. A. Ackerman, and K. N. Liou, 2004: Remote sensing of liquid water and ice cloud optical thickness and effective radius in the Arctic: Application of airborne multispectral MAS data. *J. Atmos. Oceanic Technol.,* **21,** 857–875.

Liang, S. L., and Coauthors, 2002: Validating MODIS land surface reflectance and albedo products: Methods and preliminary results. *Remote Sens. Environ.,* **83,** 149–162.

Marshak, A., S. Platnick, T. Varnai, G. Wen, and R. F. Cahalan, 2006: Impact of three-dimensional radiative effects on satellite retrievals of cloud droplet sizes. *J. Geophys. Res.,* **111,** D09207, doi:10.1029/2005JD006686.

Matsui, T., A. Beltran-Przekurat, R. A. Pielke Sr., D. Niyogi, and M. Coughenour, 2007: Continental-scale multiobservation calibration and assessment of Colorado State University Unified Land Model by application of Moderate Resolution Imaging Spectroradiometer (MODIS) surface albedo. *J. Geophys. Res.,* **112,** G02028, doi:10.1029/2006JG000229.

Moody, E. G., M. D. King, S. Platnick, C. B. Schaaf, and F. Gao, 2005: Spatially complete global spectral surface albedos: Value-added datasets derived from *Terra* MODIS land products. *IEEE Trans. Geosci. Remote Sens.,* **43,** 144–158.

Penuelas, J., and Coauthors, 2004: Complex spatiotemporal phenological shifts as a response to rainfall changes. *New Phytol.,* **161,** 837–846.

Platnick, S., M. D. King, S. A. Ackerman, W. P. Menzel, B. A. Baum, J. C. Riédi, and R. A. Frey, 2003: The MODIS cloud products: Algorithms and examples from *Terra*. *IEEE Trans. Geosci. Remote Sens.,* **41,** 459–473.

Ramon, D., and R. Santer, 2005: Aerosol over land with MERIS, present and future. *Proc. MERIS–AATSR Workshop* (ESA SP-597), Frascati, Italy, ESRIN, 9.1

Reed, B. C., J. F. Brown, D. VanderZee, T. R. Loveland, J. W. Merchant, and D. O. Ohlen, 1994: Measuring phenological variability from satellite imagery. *J. Veg. Sci.,* **5,** 703–714.

Roy, D. P., P. Lewis, C. B. Schaaf, S. Devadiga, and L. Boschetti, 2006: The global impact of clouds on the production of MODIS bidirectional reflectance model-based composites for terrestrial monitoring. *IEEE Geosci. Remote Sens. Lett.,* **3,** 452–456.

Schaaf, C. B., and Coauthors, 2002: First operational BRDF, al-

bedo nadir reflectance products from MODIS. *Remote Sens. Environ.,* **83,** 135–148.

Schwartz, M. D., 1998: Green-wave phenology. *Nature,* **394,** 839–840.

——, and B. C. Reed, 1999: Surface phenology and satellite sensor-derived onset of greenness: An initial comparison. *Int. J. Remote Sens.,* **20,** 3451–3457.

Sellers, P. J., D. A. Randall, G. J. Collatz, J. A. Berry, C. B. Field, D. A. Dazlich, C. Zhang, and L. Bounoua, 1996: A revised land surface parameterization (SiB2) for atmospheric GCMs. Part 1: Model formulation. *J. Climate,* **9,** 676–705.

Tegen, I., B. Heinold, M. Todd, J. Helmert, R. Washington, and O. Dubovik, 2006: Modelling soil dust aerosol in the Bodélé depressions during the BoDEx campaign. *Atmos. Chem. Phys.,* **6,** 4345–4359.

Wang, K., J. Liu, X. Zhou, M. Sparrow, M. Ma, Z. Sun, and W. Jiang, 2004: Validation of the MODIS global land surface albedo product using ground measurements in a semidesert region on the Tibetan Plateau. *J. Geophys. Res.,* **109,** D05107, doi:10.1029/2003JD004229.

Wen, G., A. Marshak, and R. F. Cahalan, 2006: Impact of 3-D clouds on clear-sky reflectance and aerosol retrieval in a biomass burning region of Brazil. *Geosci. Remote Sens. Lett.,* **3,** 169–172.

White, M. A., P. E. Thornton, and S. W. Running, 1997: A continental phenology model for monitoring vegetation responses to interannual climatic variability. *Global Biogeochem. Cycles,* **11,** 217–234.

Whitlock, C. H., and Coauthors, 1995: First global WCRP shortwave surface radiation budget dataset. *Bull. Amer. Meteor. Soc.,* **76,** 905–922.

Yu, H., and Coauthors, 2006: A review of measurement-based assessments of the aerosol direct radiative effect and forcing. *Atmos. Chem. Phys.,* **6,** 613–666.

Zhang, S., M. A. Friedl, C. B. Schaaf, A. H. Strahler, J. C. F. Hodges, F. Gao, B. C. Reed, and A. Huete, 2003: Monitoring vegetation phenology using MODIS. *Remote Sens. Environ.,* **84,** 471–475.

Zhang, Y., W. B. Rossow, and P. W. Stackhouse Jr., 2007: Comparison of different global information sources used in surface radiative flux calculation: Radiative properties of the surface. *J. Geophys. Res.,* **112,** D01102, doi:10.1029/2005JD007008.